Identification and analysis of atmospheric states and associated cloud properties for Darwin, Australia

S. M. Evans,[1,2] R. T. Marchand,[1,2] T. P. Ackerman,[1,2] and N. Beagley[3]

Received 13 October 2011; revised 18 January 2012; accepted 30 January 2012; published 21 March 2012.

[1] An iterative automated classification technique that combines European Centre for Medium-Range Weather Forecasts analysis data and vertically pointing millimeter wavelength cloud radar observations is used to identify commonly occurring atmospheric patterns or states around Darwin, Australia. The technique defines the atmospheric states by large-scale, synoptic variables such that, once defined, these states will be suitable to composite climate model output. Radar observations of clouds are used to test the statistical significance of each state and prompt the automated refinement of the states until each state produces a statistically stable and unique hydrometeor occurrence profile. The technique identifies eight atmospheric states: two monsoon states, two transition season states, and four dry season states. The two monsoon states can be identified as the active monsoon and the break monsoon. Among the dry season states, periods of isolated and suppressed convection can be identified. We use these states as the basis for compositing hydrometeor occurrence, precipitation rate, outgoing longwave radiation, and Madden-Julian Oscillation phase to further understand the meteorology of each state.

Citation: Evans, S. M., R. T. Marchand, T. P. Ackerman, and N. Beagley (2012), Identification and analysis of atmospheric states and associated cloud properties for Darwin, Australia, *J. Geophys. Res.*, *117*, D06204, doi:10.1029/2011JD017010.

1. Introduction

[2] General circulation models (GCMs) have difficulty representing clouds and cloud impacts on climate. This is because, in large part, the processes which control the creation, dissipation, and radiative properties of clouds occur on scales much smaller than the typical resolution of a GCM. The inability to explicitly resolve cloud processes necessitates the use of parameterizations to make statistical predictions of cloud properties. Given the broad variety and complexity of clouds found in nature, it is not surprising that these parameterizations produce errors in the statistical distributions of cloud properties when compared to observations. Determining the sources of errors in the parameterizations can be challenging, especially in GCMs [*Jakob*, 2010]. Unlike numerical weather prediction models, GCMs do not predict the specific sequence of weather events that any given location experiences, which makes it difficult to directly compare model output to observations at a particular time. A common way of addressing this problem is to create long-term temporal averages of both model output and observations, which can then be compared to each other. While comparison of long-term temporal averages can frequently determine the presence of errors, it conflates the errors that are produced when the model fails to represent the distribution of synoptic scale conditions correctly with those produced by a misrepresentative cloud parameterization. Temporal averages also do not provide much information regarding the meteorological conditions that lead to the occurrence of the errors. Information regarding the specific weather types that contribute most to the errors is lost to the averaging process.

[3] An alternate approach is to composite data by atmospheric state, rather than by season. Comparing model output with observations by atmospheric state allows for the separation of errors due to modeling of the synoptic conditions and errors due to the cloud parameterization. Comparison of the relative frequency of atmospheric states in models and in observations provides information regarding how well the model represents the state of the atmosphere. Comparing modeled cloud properties with observed cloud properties within a particular state can help detect parameterization errors; in addition, when an error is detected, the meteorological conditions which caused the error are to some degree known.

[4] There are a variety of ways of defining atmospheric states. One way is to use a particular weather variable, for example, 500 mbar vertical velocity, as a basis for compositing observations and model output [e.g., *Bony and Dufresne*, 2005]. Another method applies a clustering algorithm or principal component analysis to a set of weather observations obtained, for example, from radiosondes [*Pope et al.*, 2009; *Živković and Louis*, 1992] or reanalysis [*Fereday*

[1]Department of Atmospheric Sciences, University of Washington, Seattle, Washington, USA.
[2]Joint Institute for the Study of the Atmosphere and Ocean, Seattle, Washington, USA.
[3]Pacific Northwest National Laboratory, Richland, Washington, USA.

0148-0227/12/2011JD017010

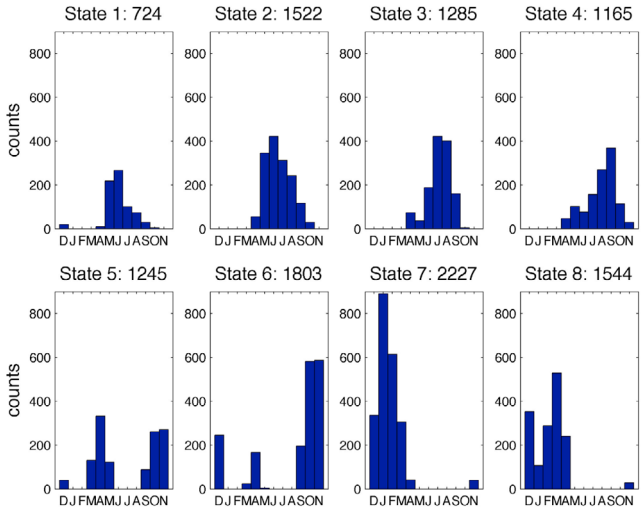

Figure 1. Monthly histograms of the occurrence of each state. The number in each panel's title indicates the total number of occurrences of each state.

et al., 2008; *Marchand et al.*, 2006; *Marchand et al.*, 2009]. Recently, clustering approaches have also been applied to cloud observations, such as those provided by the International Satellite Cloud Climatology Project (ISCCP), to create cloud regimes which can also be used to characterize regional cloud and radiative properties [*Jakob et al.*, 2005; *Jakob and Schumacher*, 2008; *Rossow et al.*, 2005], and evaluate GCM output [*Zhang et al.*, 2005; *Williams and Webb*, 2007].

[5] In this study we apply a classification technique developed by *Marchand et al.* [2009] (hereafter M09) to a region centered on Darwin, Australia. Our interest in this technique stems from its use of a combination of reanalysis and radar observations. An unresolved issue for most clustering or classification techniques is trying to determine how many states exist. In the M09 approach, the classification is applied to the reanalysis data and associated radar observations are used to ensure that the identified atmospheric states are statistically meaningful. This method, which was previously applied at the Department of Energy's (DOE) Atmospheric Radiation Measurement (ARM) program site in Oklahoma, is described in section 2, along with the input data. In M09 the technique performed well in general, but struggled to distinguish states during the summer months, suggesting that convectively dominated atmospheres may be difficult to classify with this technique. In order to test the method's capability in convective atmospheres, we opted to apply it in the tropics, again choosing an ARM site because of the presence of a cloud radar. The ARM program has sites in Darwin, Manus Island, and Nauru; the Darwin site provides the most complete radar record of the three, so we use it for our analysis.

[6] We find eight robust atmospheric states for the region surrounding Darwin, each of which can be coherently described in terms of its meteorology. We describe the meteorology of each state, their associated cloud profiles, and their seasonality in section 3. Section 4 describes the results of compositing other meteorological variables according to the atmospheric states. In section 5, we discuss future applications of our work, and compare our states to those described by *Pope et al.* [2009], who performed a clustering analysis on wet season radiosonde data from Darwin. We discuss the sensitivity of our results to a variety of design parameters in Appendix A.

2. Methods

[7] Our classification approach is described in detail in M09 and only briefly summarized here. The approach has two stages. In the first stage, meteorological variables from a numerical weather prediction analysis are input to a competitive neural network. In this study we use 3-hourly ECMWF reanalysis data from June 2006 through April 2010. Following M09, we extract relative humidity, temperature, and the horizontal winds at seven predetermined (sigma) pressure levels as well as the surface pressure for 81 horizontal grid points, arranged in a 9×9 grid centered on the ARM Darwin site. Each grid box covers an area of $2^\circ \times 2.5^\circ$ for a total of 2349 input variables at each time step. We examined the sensitivity of the results to the input data set by changing the input variables, domain size, and horizontal resolution, but found that these did not significantly alter the results. We describe in greater detail the results of these tests as well as some additional sensitivity tests we plan to undertake as part of future research in section 5.

[8] The neural network divides the input data into a predefined number of atmospheric states, where an atmospheric state may be thought of as a frequently occurring dynamic and thermodynamic pattern. Each state represents a group, or cluster, of similar observations. Essentially, each atmospheric state describes a specific weather pattern that is representative of a large number of observations. We begin by instructing the neural network to define 15 states. Mathematically, each state is defined by a vector of meteorological values for each of the input variables. To the neural network, the best representation of the input space is given by the set of state definitions such that the sum of the distances between each input vector (i.e., the meteorological variables at each time step) and the closest state definition is minimized. Distance is defined as the sum of the absolute values of the input vector elements minus the same elements in the state definition relative to the standard deviation of each element (calculated from the entire input set). As the above definition suggests, each meteorological observation (the complete set of input variables at a particular time step) is associated with the closest atmospheric state definition, which then determines the members of each cluster.

[9] In the second stage, the atmospheric states are evaluated to determine if the state has cloud properties that are temporally stable and distinct from every other state. In order for the identified atmospheric states to be useful in the analysis of climate model cloud properties, we require that the associated distribution of observed cloud properties is statistically stable. This implies that every time the state occurs the observed cloud properties may be thought of as a random realization taken from a fixed distribution. We evaluate temporal stability by comparing the mean profile of hydrometeor occurrence in the first half of the data set with that from the second half of the data set. Hydrometeor profiles are created by aggregating ARM millimeter wavelength cloud radar observations of reflectivity [*Clothiaux et al.*, 2000] according to the atmospheric states. The profiles are

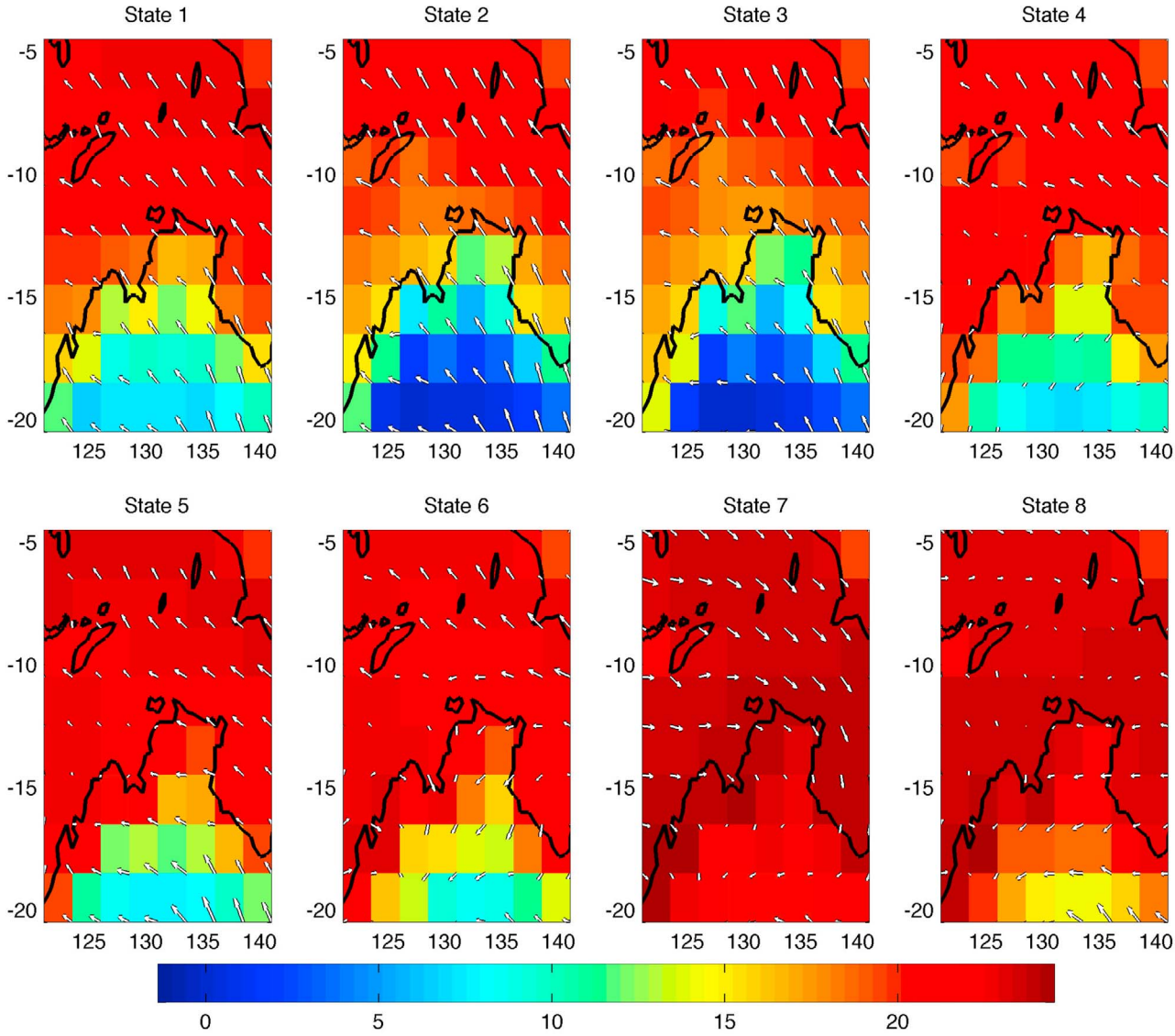

Figure 2. Surface dew points (°C) and surface wind vectors for the eight atmospheric states. Black lines show the land-sea boundaries. Latitude and longitude are labeled on the axes. Darwin is at the center of the domain.

compared using a statistical hypothesis test based on a moving-blocks bootstrap resampling technique [*Marchand et al.*, 2006]. If the hydrometeor occurrence profile in the first half of the data set differs statistically from the second half, then that state is either divided into two parts (increasing the total number of states by one) or eliminated (reducing the total number of states by one). If all the states are found to be stable, then a second test is applied, requiring that each state's hydrometeor occurrence profile be distinct from the others. Again, states that fail this test are either divided or eliminated. The process of dividing or eliminating states is repeated until all of the remaining states are temporally stable and distinct. The decision on whether to divide or eliminate a particular state is based on the size of the state. In M09 a threshold of 6% of the total number of observations was used. In this study, we found we had to increase the threshold to 7% in order for the process to converge consistently. We explain below what we mean by consistently, and discuss the role of the size threshold in greater detail in Appendix A.

[10] The results of the competitive neural network (stage 1) are slightly dependent on the order in which input is presented to the neural network as well as the iterative state refining process (stage 2). In order to test for robustness, we ran the classification process ten times with different random seed values and looked for states that occurred often. Each of the ten runs produced eight to ten states, most of which had a close match in most of the runs. To objectively determine which states were robust, we performed a cluster analysis on all of the states produced by all 10 runs. We varied the number of clusters for this stage from 8 to 12 as we looked to maximize the number of clusters that are robust, defined to be a cluster that has members from at least eight of the ten runs. The largest number of robust clusters we were able to create is 8. We mapped all the observations into these 8 states, and their means are the state

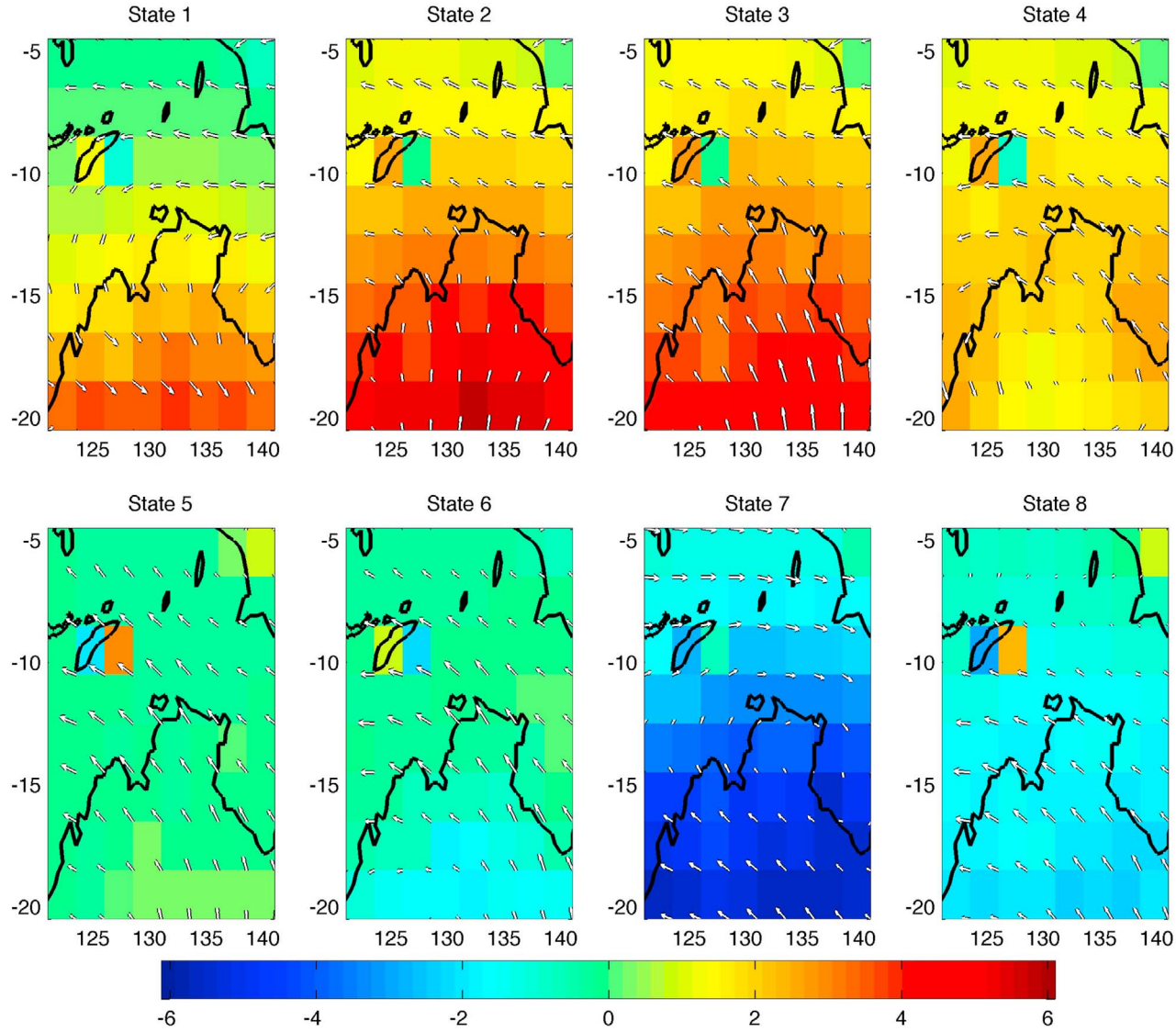

Figure 3. Surface pressure anomalies (mbar) and 750 mbar wind vectors for the eight atmospheric states. Anomalies are calculated from the mean of the full input data set. Black lines show the land-sea boundaries. Latitude and longitude are labeled on the axes. Darwin is at the center of the domain.

definitions described throughout this paper. The requirement that each state occur repeatedly means that, although the eight states presented here are not identically reproduced in each run of the classifier, the eight states comprise a good representation of the possible outcomes of the classifier. The states that were not found to be robust are briefly discussed in Appendix A.

3. Meteorology of the Atmospheric States

[11] In the remainder of this paper, we refer to the eight robust states by number, although these numbers are arbitrary, and have been assigned so as to present the states in a logical order. Darwin has a well defined monsoon climate with a dry season from May through September (approximately), monsoon season from December to March, and transitions periods in April and October–November. As shown in Figure 1, States 1–4 are dry season states, States 5 and 6 are transition season states, and States 7 and 8 are monsoon season states. The mean meteorological characteristics of each state are shown in Figure 2 for the surface dew points and winds, in Figure 3 for the surface pressure anomalies and 750 mbar winds, and in Figure 4 for the 500 mbar relative humidity and winds. Figure 5 shows the mean profile of hydrometeor occurrence (from the ARM millimeter cloud radar) for each of the eight states, showing that the two monsoon season states have more clouds and precipitation than any of the dry or transitional states. Collectively, Figures 1–5 show a clear delineation between the hot, moist monsoon season, characterized by local ascent, and the cooler, dry season, characterized by local descent.

3.1. Dry Season States

[12] States 1–4 occur nearly exclusively during the months of April to September. While all four states occur in all months of the dry season, they peak in occurrence at

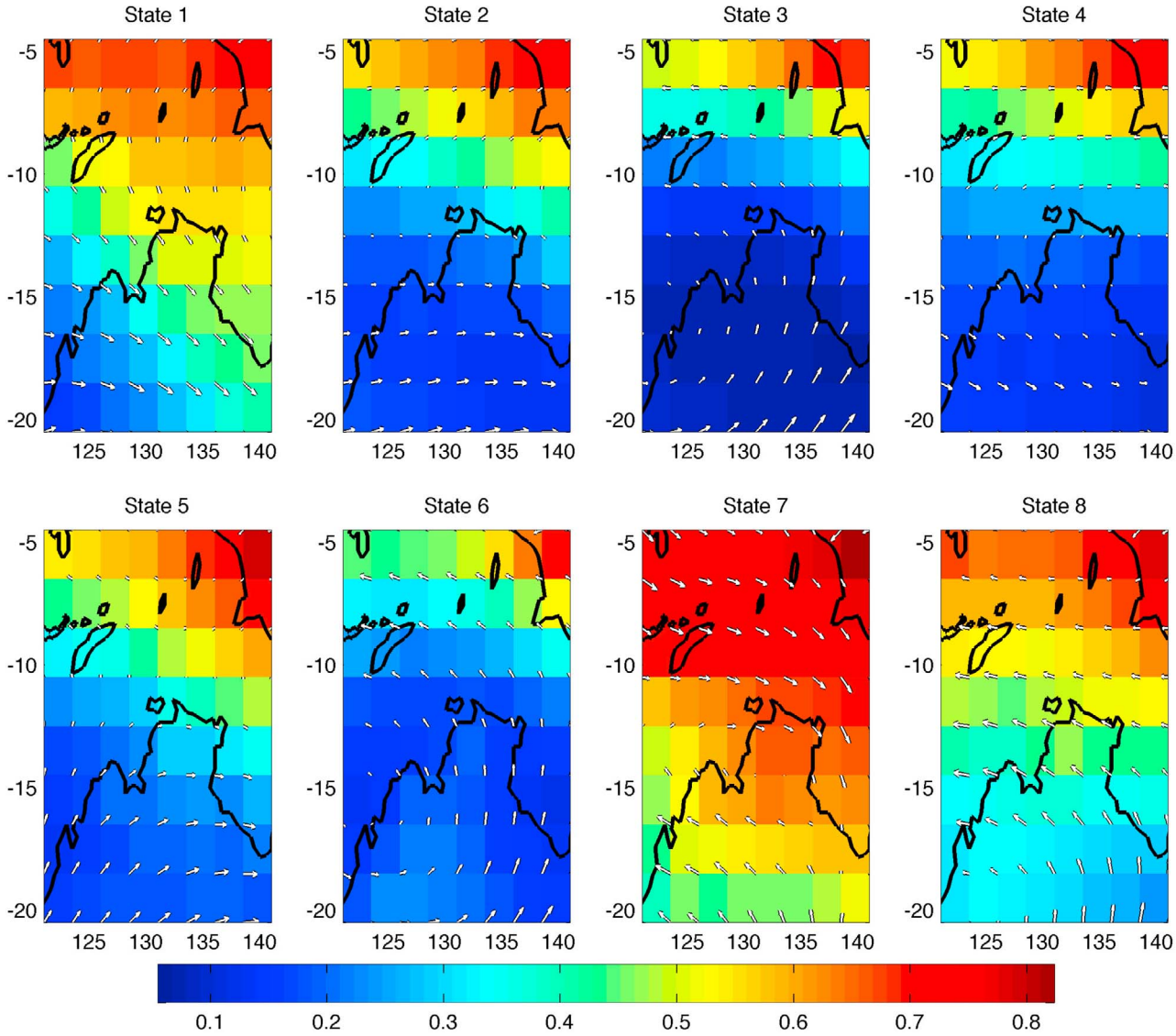

Figure 4. The 500 mbar relative humidity and 500 mbar wind vectors for the eight atmospheric states. Black lines show the land-sea boundaries. Latitude and longitude are labeled on the axes. Darwin is at the center of the domain.

different times during the season (Figure 1). States 1 and 2 occur most frequently toward the beginning of the dry season, peaking in occurrence during the months of May and June. State 3 is most common in the heart of the dry season during July and August. State 4 becomes increasingly common as the dry season winds down and the monsoon begins to build, peaking in September and continuing to occur, albeit infrequently, in October and November. The four dry season states have a number of features in common. They all have positive surface pressure anomalies (Figure 3) throughout the region, with a gradient from higher pressure in the south to lower pressure in the north. In addition, they all exhibit generally southeasterly flow at the surface (Figure 2) and anticyclonic flow in the upper atmosphere, but they have significantly different winds above the Darwin site.

[13] State 1 is a suppressed convection state. While still positive, it has the weakest surface pressure anomaly of the dry season states. At 750 mbar the flow is easterly at Darwin, while at 500 mbar the flow has reversed itself completely to become northwesterly. This northwesterly flow brings moisture from the equator, resulting in upper level humidities that are much greater than those of the other dry season states (Figure 4). State 1 is the cloudiest of the dry season states, with most of its cloud occurring below 7 km (Figure 5) suggesting little deep convection.

[14] States 2 and 3 are the driest states, with State 2 being merely dry and State 3 being very dry. Both have strongly positive surface pressure anomalies, large dew point depressions at the surface and low humidities in the upper atmosphere. States 2 and 3 are differentiated primarily by their 500 mbar flow (Figure 4). At 500 mbar, State 2 has almost no meridional component, with easterlies over the Indonesian seas, westerlies over the continent, and weak flow at Darwin. The 500 mbar flow of State 3 has lower humidities and a much stronger meridional

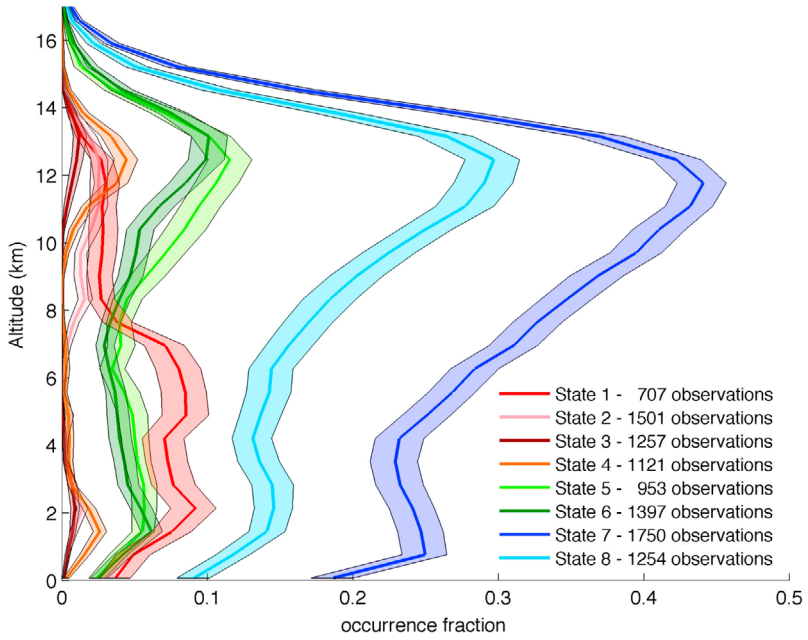

Figure 5. Vertical profiles of hydrometeor occurrence by atmospheric state, defined as the fraction of the time clouds or precipitation are detected with a reflectivity of −40 dBZ or larger by the millimeter wavelength cloud radar at the Atmospheric Radiation Measurement (ARM) site in Darwin. Dry season states are shown in shades of red, transition states are in green, and monsoon states are in blue. Shaded areas denote the 95% confidence limits, as determined by the bootstrap resampling method. The numbers in the legend indicate the number of 3 h blocks with radar observations for each state, which are not precisely the same as the number of reanalysis observations shown in Figure 1.

component at Darwin, with southwesterly flow over the continent providing an anticyclonic pattern over the region. State 2 produces a very small amount of cloud, primarily above 7 km. State 3 produces almost no cloud at all.

[15] State 4 is an isolated convection state, as will become clearer in section 4 when we examine precipitation. It has little gradient in its surface pressure field and its surface flow is easterly at Darwin. The surface flow diverges when it reaches the continent, producing northeasterly winds over the continental interior that are similar to the flow in the monsoon states. Its surface temperatures are nearly as hot as those of the monsoon season states (not shown), making it by far the hottest of the dry season states. While not nearly as moist as State 1, it is still more humid than either State 2 or State 3, and features a bimodal cloud height distribution with distinct peaks near 1.5 and 12 km. As the changes in surface temperature and flow suggest, this state occurs most often toward the end of the dry season and buildup to the monsoon.

3.2. Transition Season States

[16] States 5 and 6 both occur primarily during the months of March to May and September to November (Figure 1). State 5 occurs approximately equally in both shoulder seasons, while State 6 occurs almost entirely in the premonsoon transition, and continues to occur, somewhat less frequently, into December. Both states have high surface temperatures equal to those of the monsoon season (not shown) but drier humidity profiles that are similar to dry season states (see for example at 500 mbar, Figure 4). State 5 is somewhat more humid, while State 6 is slightly hotter (not shown). Both states have close to neutral surface pressure anomalies with weak gradients. The two states are most readily distinguished by their flow patterns. At Darwin, State 5 is southeasterly at the surface and at 750 mbar (Figures 2 and 3) before becoming southwesterly at 500 mbar (Figure 4). State 6 has primarily easterly flow at the surface, although there is westerly onshore flow on the western coast of the continent. At 500 mbar, State 6 features strong southeasterly flow at Darwin with a strong anticyclone centered in the western part of the domain. States 5 and 6 have very similar hydrometeor occurrence profiles (Figure 5); however, the statistical analysis shows that the larger hydrometeor occurrence around 10 km in State 5 is significant at the 95% confidence interval, which is consistent with higher upper level humidity. In both states, the profiles are double peaked at approximately 2 and 13 km, with greater occurrence than the dry season states and much less than the monsoon states.

3.3. Monsoon Season States

[17] States 7 and 8 are monsoon season states, occurring almost entirely between December and April (Figure 1). State 7 occurs more frequently in January and February, the core of the monsoon season, and represents the monsoon during its most active phase. State 8 occurs more often on the edges of the monsoon season in December and March and represents a break monsoon condition. Both have high surface temperatures, high humidities, and negative surface pressure anomalies. They differ in their flow patterns however. At Darwin, State 7 has westerly, slightly cyclonic flow

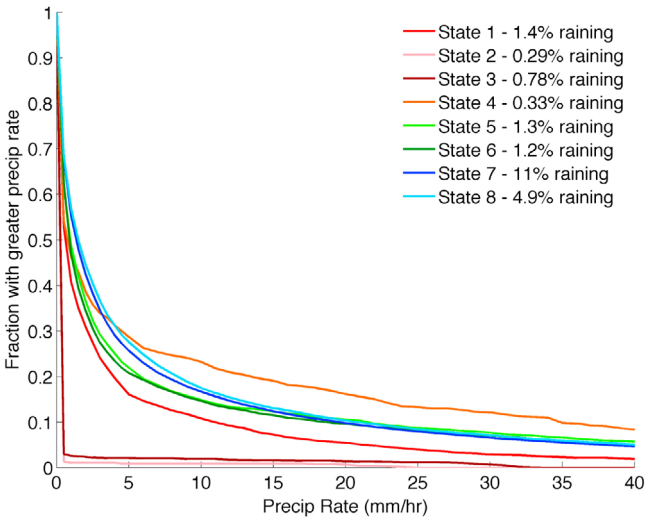

Figure 6. Cumulative occurrence of precipitation rate for each of the atmospheric states. Precipitation rates come from the rain gauge at the ARM site in Darwin. Only data from times when there was rain are used in the calculation. The legend indicates the percent of the time it was raining for each state, e.g., the dark blue line represents 11% of State 7. Colors are the same as in Figure 5, with red shades representing dry season states, green representing transitional states, and blue representing monsoon states.

at the surface, which becomes strongly cyclonic and slightly northwesterly at 500 mbar. The strong and moist onshore flow makes State 7 the most humid of all the states. State 8 has easterly flow at the surface which becomes anticyclonic by 500 mbar. In this way it resembles a more humid version of State 6, although the center of the anticyclone is further south. States 7 and 8 are the cloudiest and second-cloudiest states, respectively, with a primary peak in the occurrence profile at 12 km, and a smaller peak at approximately 2 km (Figure 5).

4. Additional Variables Associated With the Atmospheric States

[18] Using the state definitions and associated time series, we can now composite a variety of other observations by state. We are particularly interested in cloud properties and precipitation for the sake of future comparison to model output. Precipitation data come from the tipping bucket rain gauge at the ARM site. Outgoing longwave radiation (OLR) data was obtained from the CERES [*Wielicki et al.*, 1996] SYNlite Ed2.5 product (D. Doelling et al., manuscript in preparation, 2012), which employed the geostationary enhanced temporal interpolation method to model the OLR hourly signal in between CERES measurements. The hourly resolution was provided by the CERES team for the 1° latitude/longitude region over Darwin as the official SYNlite Ed2.5 product does not contain hourly fluxes. We also investigate the relationship between state occurrence and the phase of the Madden-Julian Oscillation (MJO). Here we use the definition of MJO phase described by *Wheeler and Hendon* [2004] and provided by the Australian Bureau of Meteorology Research Centre.

4.1. Precipitation

[19] Figure 6 shows cumulative occurrence curves of rain rates for each state, calculated only for times when precipitation is detected. The values for rain rate are the means of all the nonzero values within 1.5 h of the ECMWF analysis times. These curves represent the cumulative occurrence when it is raining during a particular state, rather than fractional occurrence during all times. The percentage of observations with rain is shown in the legend. Thus, the curve for State 7, which rains most frequently, represents 11% of the observations from that state, while the curve for State 2 represents less than 0.3% of the observations of that state.

[20] The curves display an expected exponential behavior with varying decay rates. Generally speaking, the overall frequency of precipitation and the relative frequency of intense rain correlate, with the monsoon states raining more than the transitional states which in turn rain more than the dry season states. State 4 is a major exception, however, raining only 0.3% of the time, but raining more intensely than any other state, even the monsoon states. This observation helps to identify State 4 as a state of isolated convection, with small pockets of convection producing highly localized, intense precipitation that only occasionally passes over the ARM site. This conceptual interpretation of State 4 is consistent with the radar occurrence profile (Figure 5), which shows very few hydrometeor detections at midlevels, but a peak in upper level cloud associated with cirrus outflow from the tops of passing towers. It is also worth noting that State 1, despite having relatively frequent cloud and precipitation occurrence has relatively weak precipitation rates. This is consistent with a state of suppressed convection and a lack of high clouds.

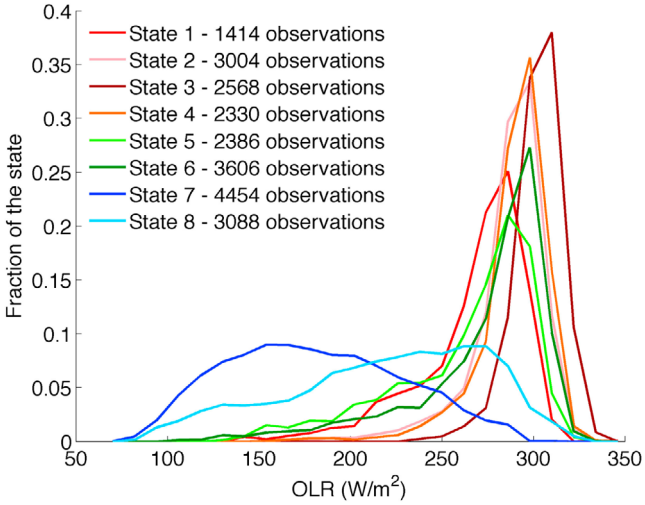

Figure 7. The distribution of outgoing longwave radiation (OLR) values for each state. Data come from the Clouds and the Earth's Radiant Energy System (CERES) SYNlite product and, in this case, represent hourly means averaged over 1 square degree. The legend indicates the number of OLR observations for each state. Colors are the same as in Figure 4, with red shades representing dry season states, green representing transitional states, and blue representing monsoon states.

Table 1. Statistics of the Distribution of Outgoing Longwave Radiation Values for Each State

State	Mean (W/m^2)	SD (W/m^2)	Skewness	Kurtosis
1	267.7	29.2	−1.4	5.4
2	286.9	19.5	−1.9	8.1
3	302.5	12.9	−1.0	5.5
4	289.3	19.9	−2.3	11.5
5	263.2	37.8	−1.2	3.8
6	273.0	37.6	−1.7	5.9
7	180.2	47.2	0.2	2.3
8	219.7	53.8	−0.5	2.4

4.2. Outgoing Longwave Radiation

[21] Figure 7 shows the distribution of observed outgoing longwave radiation (OLR) values for each state. The data are hourly means averaged over 1 square degree (100 km by 100 km) around Darwin. The statistics of these distributions are summarized in Table 1. States 7 and 8 immediately stand out because of their low average values, large standard deviations, and small skewness values, which are all consistent with the high frequency of deep clouds (Figure 5). State 7 is the only state to have a positive skewness, making it the only state where deep clouds are the norm.

[22] More subtle differences exist among the other states. The two transitional states (States 5 and 6) and the low-cloud state (State 1) have lower mean values and greater standard deviations than the other nonmonsoon states, reflecting the greater frequency of clouds for these states. The warmer surface temperatures of States 5 and 6 as compared to State 1 are also evident, as States 5 and 6 have much higher occurrence of OLR values greater than 300 W/m^2. States 2 and 4 have very similar distributions, owing to neither having clouds often. Last, State 3 has both the highest mean value and the smallest standard deviation, a reflection of the fact that it is nearly always cloud free.

4.3. MJO Phase

[23] Figure 8 shows the relative occurrence of different phases of the MJO for each state, with periods of weak MJO activity having been removed from the data. The calculation of these phases, as well as the definition of weak activity is described in detail by *Wheeler and Hendon* [2004]. Under the Wheeler and Hendon definitions, different MJO phases indicate different geographic centers of the enhanced convection associated with the MJO. Phases 8 and 1 indicate enhanced convection over the western hemisphere and Africa, phases 2 and 3 indicate enhanced convection over the Indian Ocean, phases 4 and 5 indicate enhanced convection over the maritime continent, and phases 6 and 7 indicate enhanced convection over the western Pacific. Darwin's location means it experiences enhanced convection during phases 4, 5, and 6 and suppressed convection in phases 8, 1, and 2. We show the relative occurrence of the MJO phases rather than absolute counts to account for the fact that the different phases of the MJO do not occur in equal proportion during our period of observation. We define relative occurrence as the percent difference from the expected distribution of MJO phases, where the expected distribution for a single state is the same as is observed for the full period of observation.

[24] Looking at the monsoon season states first, we can see that State 7 has a strong preference for the MJO to be present at Darwin, while State 8 prefers the MJO to be further away. This is in keeping with our interpretation of States 7 and 8 as the active and break monsoon, respectively. A similar relationship appears to happen during the transition seasons, when the presence of the MJO strongly favors State 5, while State 6 has no obvious preference. Among the dry season states, States 1 and 2 show a preference for suppressed convection associated with a distant MJO. This location of the MJO produces upper level subsidence in the Darwin area, which may be responsible for the lack of high cloud, despite high relative humidity values and extensive lower clouds in State 1. This MJO location may also explain how State 2 can rain less frequently and less intensely than State 3, despite being slightly more humid and cloudy. State 4 has a preference for MJO phase 4, in which the enhanced convection effects are just reaching Darwin. This fits with our conceptual description of State 4 as a dry, high-pressure state which still produces isolated convective activity. Overall, the correlation of the MJO with different states reinforces our interpretation of the dynamics of the states and is suggestive of a relationship between the MJO and transitions between the states, although we have not demonstrated that here.

5. Discussion

[25] Our analysis identifies eight robust atmospheric states for the region surrounding Darwin, Australia. Each state has an easily understood meteorological definition, which is

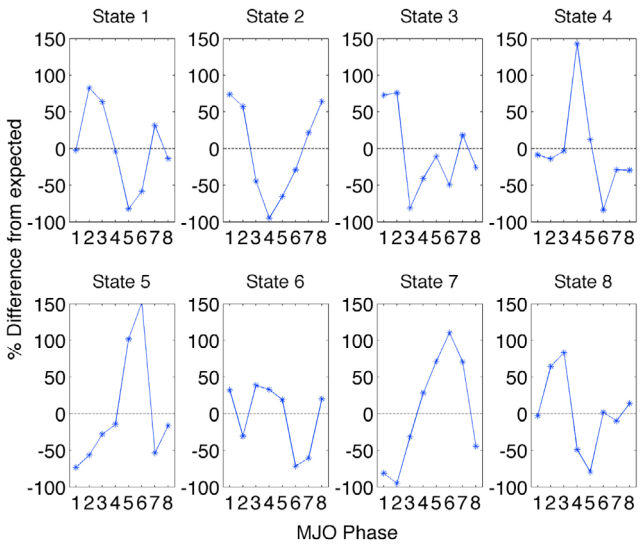

Figure 8. Distribution of MJO phase, as calculated by *Wheeler and Hendon* [2004], for each of the atmospheric states. Weakly defined phases (amplitude <1) have been removed from the data. Values are the percent difference from the expected number of occurrences of each phase. The expected number of occurrences is the overall occurrence rate of each phase during the 4 years of our study. Data were provided by the Australian Bureau of Meteorology Research Centre. In the Wheeler and Hendon definitions, Darwin is located near the boundary between phases 5 and 6.

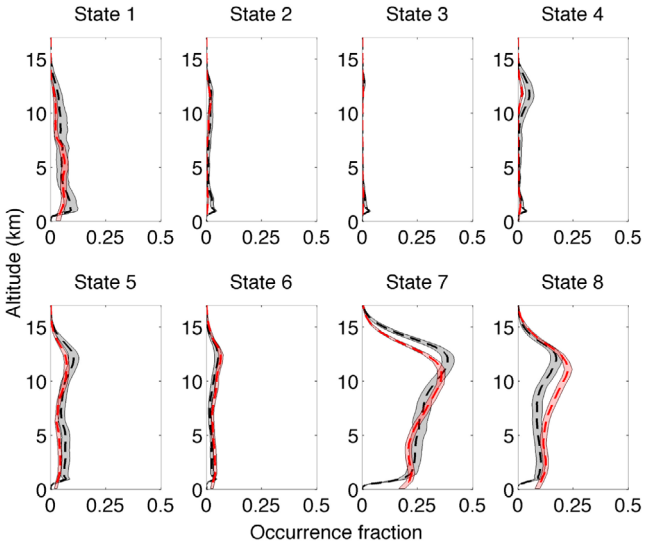

Figure 9. Cloud occurrence profiles calculated from both the millimeter radar at the ARM site in Darwin (red) and from CloudSat observations within 5° of Darwin (black). Dashed lines indicate the mean values at each altitude, and shaded regions indicate the 95% confidence limits as calculated by the bootstrap resampling method. CloudSat has larger uncertainties because of fewer observations. ARM profiles are not the same as in Figure 5 because a detection threshold of −27.5 dBZ has been applied rather than −40 dBZ in order to match the sensitivity of the CloudSat radar.

complemented by additional information regarding seasonality, hydrometeor characteristics, outgoing longwave radiation, and the phase of the MJO. Despite using very different data sets and methods, some of our states are good matches to those found by *Pope et al.* [2009], hereafter referred to as P09. P09 performed a cluster analysis on 49 years of wet season radiosonde data from Darwin to create definitions of five atmospheric states which they refer to as regimes. They use temperature and wind measurements taken at 16 vertical levels from radiosondes launched once daily during the months of September through April. Since their study does not have data for May through August, a comparison of dry season states is not possible.

[26] Both of our monsoon states find good matches among the P09 regimes. Our State 7 matches with the Deep West regime of P09, also identified as the active monsoon. The Deep West regime is westerly at Darwin up to a height of 400 mbar, while our State 7 is westerly up to 375 mbar, which is the nearest vertical level in our data set. There are some small differences in the meridional winds, as the Deep West regime is northerly up to 300 mbar, while our State 7 varies between lightly northerly and lightly southerly throughout the atmosphere. The Deep West regime has large negative OLR anomalies, consistent with the low OLR values we observe for State 7 (Figure 7). The two also occur at the same time: almost exclusively from December to March, with a peak in January and February. Our other monsoon state, State 8, is a good match to P09's Moist East regime, also identified as the monsoon break. Both are easterly throughout the column with southerly or very lightly northerly meridional winds, and occur most frequently at the edges of the monsoon season in December and March. The Moist East regime also has negative OLR anomalies associated with it, but much weaker than those of the Deep West regime, again consistent with the OLR distribution for State 8 (Figure 7). The rest of the P09 regimes are more difficult to match. The P09 Shallow West regime does not appear to have any direct counterpart in our definitions, as we have no state other than State 7 with low-level westerlies. It is likely that this regime is subsumed within our State 7. The only nonmonsoon season regimes in P09 are the Dry East and East regimes. Since these are being compared to 6 of our states covering the same period, we do not expect close matches, but rather that their states are amalgamations of our dry season states.

[27] One focus of future work involves the millimeter wavelength radar on CloudSat. Our classification technique can be modified to use CloudSat cloud radar observations in place of ARM ground-based cloud radar observations. A detailed description of the salient differences between these radars, including the effects from rain, is given by *Liu et al.* [2010]. Relevant to the discussion here is that vertical profiles of cloud occurrence from the two radars agree when aggregated on spatial scales of 4.5 to 7 degrees. Attenuation during heavy rain does cause differences in the reflectivity near the surface and in the upper troposphere, but reductions in reflectivity due to attenuation have little effect on occurrence, i.e., the detection of hydrometeors. We have composited the CloudSat radar observations in the 5° around Darwin as a function of atmospheric state. A comparison of the ARM occurrence profiles with the CloudSat profiles is shown in Figure 9. Most profiles are similar at most altitudes, but there are some differences. The greatest discrepancy between ARM and CloudSat profiles is in State 8. Investigating the contribution of different CloudSat paths to this difference led us to discover an east to west gradient in cloud cover, indicating that the cloud cover observed by ARM at Darwin is not representative of that of the larger region for this state. The differences in State 7, more hydrometeors at high altitudes when viewed by CloudSat and more at low altitudes when viewed by ARM, can be explained by considering that CloudSat is looking down from above while ARM is looking up from below. In both cases, the radars are being attenuated before they can see all the hydrometeors in the column. The attenuation of CloudSat at low altitudes is particularly evident for the monsoon states. The differences for State 4 where CloudSat shows a greater occurrence of hydrometeors at almost all altitudes, are likely attributable to the meteorology of the state. This state features isolated convection. We suggest that the CloudSat data show a greater cloud occurrence because the CloudSat data, because they are composited over a 5° region, have greater odds of observing a convective tower. While the uncertainty bounds of the CloudSat data are larger than those of ARM (because they have fewer samples), the uncertainty is sufficiently small that the CloudSat profiles remain distinct from one another. This is demonstrated in Figure 10, which shows the CloudSat profiles for each state. The larger uncertainties on the profiles lead to more overlap of the profiles than among the ground-based profiles (Figure 5), but close inspection makes it clear that every profile is in fact distinct from every other profile. We therefore conclude that we will be able to use CloudSat

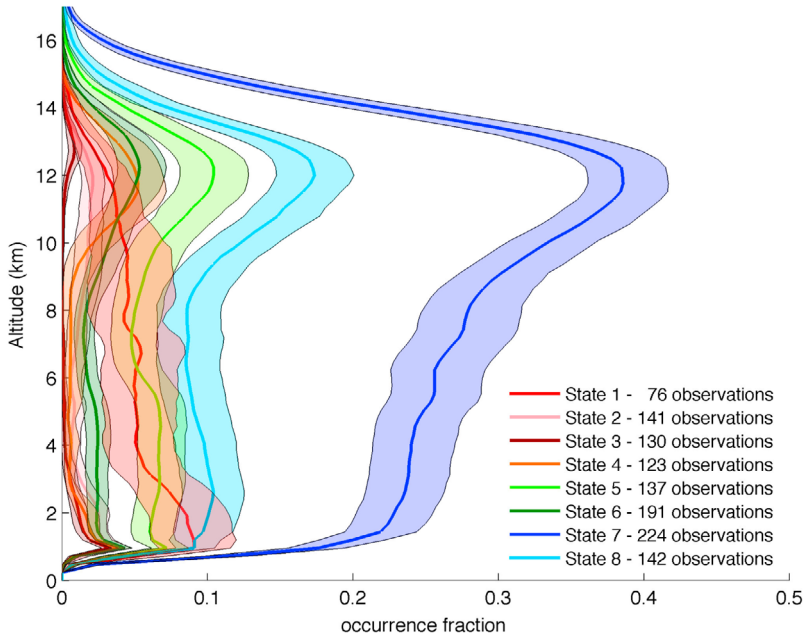

Figure 10. Vertical profiles of hydrometeor occurrence by atmospheric state, as observed by CloudSat. Occurrence is defined as the fraction of the time clouds or precipitation are detected with a reflectivity of −27.5 dBZ or larger by the cloud radar aboard CloudSat. Dry season states are shown in shades of red, transition states are in green, and monsoon states are in blue. Shaded areas denote the 95% confidence limits, as determined by the bootstrap resampling method. The numbers in the legend indicate the number of overpasses by CloudSat for each state, which are substantially smaller than the number of observations in Figure 5.

measurements in place of ARM measurements in regions in which ground-based radar data are not available.

[28] One objective of the research described in this article was to determine if the atmospheric classification technique developed by M09 could be successfully applied in a tropical location (Darwin, Australia) with the intent of developing a set of atmospheric states for Darwin that are suitable for use in comparison of climate model output with observations from the ARM site. We conclude that the classification technique does work, in the sense that it identifies a set of meteorologically identifiable patterns with statistically distinct and temporally stable cloud properties. It is worth noting, however, that results were largely insensitive to the size of the analysis domain or the horizontal resolution (see Appendix A). The monsoon states at Darwin from the M09 method are also similar in many respects to those found by P09 on the basis of clustering of radiosonde observations. This suggests that the spatial structure of the analysis fields may be adding relatively little information content to the classification and the primary benefit of including these data may be in providing a context in which to interpret the states. Alternatively, the spatial structure may be allowing us to find those states with only 4 years of data as opposed to 49 (as in P09). We expect that as we increase the length of the data set we will find more states, as the power of the statistical tests to discern small differences increases. In particular, we think that with only a slightly longer data set we will find a third monsoon state and fifth dry season state (see Appendix A). We argue that more states, so long as they remain statistically distinct, are beneficial, as we will be able to more precisely identify different weather regimes. More states overall may also result in multiple states that, while statistically distinct, appear quite similar. These can always be combined later during analysis if so desired, but we do not want to preclude the possibility of an interesting discovery by reducing the number of states during the identification stage.

[29] The M09 technique also identifies fewer total states at Darwin than was the case when this technique was applied to the U.S. Southern Great Plains, despite the fact a slightly larger data set was used in the present study. In general, we expect the classification technique to produce more states as the size of the data set increases for the simple reason that the associated statistical distinctness and stability test are more capable of identifying differences as the sampling uncertainty is reduced. While identifying fewer states at Darwin may simply be due to having less varied synoptic conditions, it is also possible that this difference reflects fundamentally lower predictability in the relationship between synoptic variables and clouds observed at a location with persistent convective conditions. We speculate that we may identify more states if our statistical analysis includes observables with greater spatial extent (such as satellite or scanning radar based cloud cover) or properties beyond simple occurrence (such as distributions of reflectivity or optical properties).

[30] Another goal of this research, as well as many other classification studies, is to provide a useful diagnostic of climate model cloud parameterizations. The M09 methodology uses analyses of atmosphere state variables at

resolutions typically associated with the large-mesoscale to synoptic scale. While cloud profiles are used to determine the statistical significance of each state, the state definitions contain only large-scale variables. Other classification methodologies [e.g., *Jakob et al.*, 2005; *Rossow et al.*, 2005] start with radiatively determined variables such as cloud optical depth and cloud top height, carry out a cluster analysis based on these variables, and then aggregate dynamical states associated with each cluster. One can view this difference from the perspective of causality. Meteorologists typically view cloud patterns and properties as the result of dynamics and thermodynamics. For example, the very useful classification of *Bony et al.* [2004] is based solely on the 500 mbar vertical velocity and correlates all cloud patterns with this single dynamical variable. GCMs and NWP models predict cloud occurrence on the basis of model dynamical and thermodynamical profiles. Clearly, clouds affect the large-scale dynamical state of the atmosphere through diabatic heating and vertical transport, but on relatively long timescales. The immediate progression is from dynamics to clouds. Our methodology adopts this causal progression by analyzing atmospheric states first and then identifying the cloud patterns associated with them. Consequently, we think that it is a worthwhile complement to those that begin with cloud radiative properties and that it permits us to provide useful comparisons with GCM states and associated cloud properties. We intend to pursue this line of research over the next few years and provide evidence of the diagnostic utility of our methodology.

Appendix A

[31] In testing whether the method from M09 could be successfully applied to the tropics, we performed a number of sensitivity tests to check whether the algorithm parameters used at SGP were still suitable. We varied the size threshold for dividing/deleting bad states, the list of input variables and their horizontal resolution, and implemented a screen for outliers. All these sensitivity tests were performed on half the data set. Here we describe the results of these tests.

[32] The size threshold used in the iteration stage affects the number of states produced by the classifier because it decides whether a bad state is eliminated or divided. Lower values for this parameter force the classifier to try to find smaller clusters by more frequently choosing to subdivide rather than eliminate states. However, if one tries to find more states than can be supported by the data, then the classifier struggles to converge. For example, if a good state is artificially divided into two parts, both halves will likely have similar (i.e., nondistinct) cloud profiles causing the division to be rejected. Thus, the goal when setting the threshold value is to set it as low as possible (in order to obtain as many good states as possible) while still achieving convergence on a set of stable and distinct states. In M09 this value was set at 6% of the total number of observations. Here, we set it to 7% after determining that this is the lowest value at which the classifier still converged on a set of states. The larger value used here for Darwin reflects the fact that fewer atmospheric states exist (or at least can be robustly identified for the specific statistical test employed) in the tropics as compare to the midlatitudes.

[33] Another design choice which might affect the results is the selection of the input data. To test this, we ran the classifier multiple times on data sets with a number of variations from the standard case we have described throughout this paper. We tested for the importance of variable selection by adding either geopotential height or divergence to the list of variables extracted from the ECMWF reanalysis and tested for the importance of domain size by expanding our grid of points from 9×9 to 9×18 and shrinking it to 5×5. We also tested the importance of horizontal resolution, by creating data sets that covered the same regions as the base case, but at $1^\circ \times 1^\circ$ resolution and $0.5^\circ \times 0.5^\circ$ resolution. All six of these variants produced very similar results to those described in section 3.

[34] In section 2, we mentioned that individual runs sometimes produced nonrobust states (that is states which did not have a close match in at least 8 of 10 runs). These nonrobust states came in two forms, one as an additional monsoon state and the other as an additional dry season state. When an additional monsoon state is created, it is produced by taking members from both States 7 and 8 and creating a new state different from either. This additional state, which is not shown here, has similar surface traits to State 7, but 500 mbar flow that is northeasterly rather than the northwesterly of State 7 or the southeasterly of State 8. The hydrometeor profile of this state is intermediate between States 7 and 8. More rarely, a fifth dry season state was found. It was typically a mix of elements from States 1 and 2, with meteorology and cloud profile intermediate between the two. Given a larger input data set, it is possible that one or both of these states may become robust, but as it stands neither occurs frequently enough to be reliably identified as an atmospheric state.

[35] We also investigated the extent to which our states are affected by outlier observations. Presently, a state is defined as the mean of all its members, and all observations are assigned to a state. Some observations, however, are poor matches for any of the states, but our methodology forces them into a state and to contribute to the overall statistics. We experimented with removing the 5% most outlying observations from each state and recalculating the statistics for each state. By doing so, we were essentially adding a requirement that states be relatively tightly clustered near the centroid. We found however, that removing the outliers from each state did not notably alter the statistics for each state. As such, it appears that the state definitions are not strongly affected by outliers.

[36] **Acknowledgments.** We thank Philip Partain (Colorado State University), the CloudSat project participants, and ECMWF for providing the CloudSat radar observations and ECMWF analysis data. We thank David Doelling (NASA Langley Research Center) for providing CERES data. We also thank the many Atmospheric Radiation Measurement (ARM) instrument mentors and data archivists for all their efforts in producing and maintaining the quality of the ARM data sets. This research was supported by NASA (ROSES) under contract NNX07AR98G S05, the U.S. Department of Energy Atmospheric System Research program under contract DESC0002472, and Pacific Northwest National Laboratory award 39189.

References

Bony, S., and J.-L. Dufresne (2005), Marine boundary layer clouds at the heart of tropical cloud feedback uncertainties in climate models, *Geophys. Res. Lett.*, *32*, L20806, doi:10.1029/2005GL023851.

Bony, S., J.-L. Dufresne, H. Le Treut, J.-J. Morcrette, and C. Senior (2004), On dynamic and thermodynamic components of cloud changes, *Clim. Dyn.*, *22*, 71–86, doi:10.1007/s00382-003-0369-6.

Clothiaux, E. E., T. P. Ackerman, G. G. Mace, K. P. Moran, R. T. Marchand, M. A. Miller, and B. E. Martner (2000), Objective determination of cloud heights and radar reflectivities using a combination of active remote sensors at the ARM CART sites, *J. Appl. Meteorol.*, *39*, 645–665, doi:10.1175/1520-0450(2000)039<0645:ODOCHA>2.0.CO;2.

Fereday, D. R., J. R. Knight, A. A. Scalfe, and C. K. Folland (2008), Cluster analysis of North Atlantic–European circulation types and links with tropical Pacific sea surface temperatures, *J. Clim.*, *21*, 3687–3703, doi:10.1175/2007JCLI1875.1.

Jakob, C. (2010), Accelerating progress in global atmospheric model development through improved parameterizations: Challenges, opportunities, and strategies, *Bull. Am. Meteorol. Soc.*, *91*, 869–875, doi:10.1175/2009BAMS2898.1.

Jakob, C., and C. Schumacher (2008), Precipitation and latent heating characteristics of the major tropical western Pacific cloud regimes, *J. Clim.*, *21*, 4348–4364, doi:10.1175/2008JCLI2122.1.

Jakob, C., G. Tselioudas, and T. Hume (2005), The radiative, cloud, and thermodynamic properties of the major tropical western Pacific cloud regimes, *J. Clim.*, *18*, 1203–1215, doi:10.1175/JCLI3326.1.

Liu, Z., R. Marchand, and T. Ackerman (2010), A comparison of observations in the tropical western Pacific from ground-based and satellite millimeter-wavelength cloud radars, *J. Geophys. Res.*, *115*, D24206, doi:10.1029/2009JD013575.

Marchand, R., N. Beagley, S. E. Thompson, T. Ackerman, and D. Schultz (2006), A bootstrap technique for testing the relationship between local-scale radar observations of cloud occurrence and large-scale atmospheric fields, *J. Atmos. Sci.*, *63*, 2813–2830, doi:10.1175/JAS3772.1.

Marchand, R., N. Beagley, and T. Ackerman (2009), Evaluation of hydrometeor occurrence profiles in the Multiscale Modeling Framework climate model using atmospheric classification, *J. Clim.*, *22*, 4557–4573, doi:10.1175/2009JCLI2638.1.

Pope, M., C. Jakob, and M. Reeder (2009), Regimes of the north Australian wet season, *J. Clim.*, *22*, 6699–6715, doi:10.1175/2009JCLI3057.1.

Rossow, W. B., G. Tselioudas, A. Polak, and C. Jakob (2005), Tropical climate described as a distribution of weather states indicated by distinct mesoscale cloud property mixtures, *Geophys. Res. Lett.*, *32*, L21812, doi:10.1029/2005GL024584.

Wheeler, M., and H. Hendon (2004), An all-season real-time multivariate MJO index: Development of an index for monitoring and prediction, *Mon. Weather Rev.*, *132*, 1917–1932, doi:10.1175/1520-0493(2004)132<1917:AARMMI>2.0.CO;2.

Wielicki, B. A., B. R. Barkstrom, E. F. Harrison, R. B. Lee III, G. L. Smith, and J. E. Cooper (1996), Clouds and the Earth's Radiant Energy System (CERES): An Earth Observing System experiment, *Bull. Am. Meteorol. Soc.*, *77*, 853–868, doi:10.1175/1520-0477(1996)077<0853:CATERE>2.0.CO;2.

Williams, K. D., and M. J. Webb (2007), A quantitative climate performance assessment of cloud regimes in GCMs, *Clim. Dyn.*, *29*, 231–250, doi:10.1007/s00382-007-0232-2.

Zhang, M. H., et al. (2005), Comparing clouds and their seasonal variations in 10 atmospheric general circulation models with satellite measurement, *J. Geophys. Res.*, *110*, D15S02, doi:10.1029/2004JD005021.

Živković, M., and J.-F. Louis (1992), A new method for developing cloud specification schemes in general circulation models, *Mon. Weather Rev.*, *120*, 2928–2941, doi:10.1175/1520-0493(1992)120<2928:ANMFDC>2.0.CO;2.

T. P. Ackerman, S. M. Evans, and R. T. Marchand, Department of Atmospheric Sciences, University of Washington, 408 ATG Bldg., Box 351640, Seattle, WA 98195-1640, USA. (sevans@atmos.washington.edu)

N. Beagley, Pacific Northwest National Laboratory, PO Box 999, Richland, WA 99352, USA.